Supporting Information

Ultralong Room Temperature Phosphorescence with Multicolor Afterglow Achieved in Harsh Polymeric Viscous Flow State

Shiyu Gu, *Qi Wu** & *Jinrong Wu**

College of Polymer Science and Engineering, Stake Key Laboratory of Polymer Materials Engineering, Sichuan University, Chengdu 610065, People's Republic of China.

* Corresponding E-mail: wuqi57@scu.edu.cn (Q.W.) and wujinrong@scu.edu.cn (J. W.)

This file includes:

Supplementary Text

Figure S1 to S15

Tables S1 to S7

Legends for Movies S1 to S8

Other Supplementary Materials for this manuscript include the following:

Movies S1 to S8

Supplementary Text

Synthesis Procedures

Preparation of the x% BA-PBS

BA and PDMS-OH were mixed at room temperature, and MeOH (2 ml) was added dropwise. The molar ratios of B-OH to Si-OH were 9:10, 13:10 and 18:10. Following this, the mixtures were maintained at 60 °C in a vacuum oven for 6 h to accomplish a complete B-O click reaction and remove methanol. Finally, the dried samples were labeled as x% BA-PBS (x% stood for the molar ratio of B-OH to Si-OH, and it varied from 90%, 130% and 180%, Table S1).

Preparation of the x% BA-PVA

Firstly, PVA (20 g) was dissolved in 400 ml deionized water at 90 °C and stirred for 3 h to get a PVA solution (50 mg/ml). PVA solution (10 ml, 50 mg/ml) was poured into three PTFE molds and dried at 80 °C in a vacuum oven for 4 h to get pure PVA films. Secondly, BA (120 mg, 230 mg, 350 mg) was dissolved in a mixed solvent (2 ml MeOH and 3 ml deionized water) to get BA solutions (24 mg/ml, 46 mg/ml, 70 mg/ml), respectively. Finally, pure PVA films were soaked in the BA solutions for 12 h and dried in the vacuum oven at 80 °C for 6 h to obtain dried BA-PVA films. Then, the films were labeled as x% BA-PVA (x% stood for the molar ratio of B-OH to C-OH, and it varied from 50 %, 100% and 150%, Table S2).

Preparation of the TPB-3NH_2-doped PVA and x% BA-PVA

Firstly, TPB-3NH_2 solution (2 mg/ml) was prepared by dissolving TPB-3NH_2 (40 mg) in 20 ml DMF under continuous shaking. Then, TPB-3NH_2-doped x% BA-PVA films were fabricated by blending BA solutions (24 mg/ml, 46 mg/ml, 70 mg/ml) and PVA (10 ml) with TPB-3NH_2 solution (0.5 ml). Afterward, the mixtures were poured into PTFE molds and dried in the vacuum oven at 80 °C for 6 h. The films were labeled as TPB-3NH_2-doped PVA and TPB-3NH_2-doped x% BA-PVA (x% stood for the molar ratio of B-OH to C-OH, and it varied from 50 %, 100% and 150%, Table S3).

Preparation of the RTPP-x and controlled samples

Regarding the total molar amount of hydroxyl groups in PVA and PDMS-OH as one, we prepared RTPP-x with the B-OH of 0.75, 1, 1.25 and 1.5 equivalent (x stood for the molar ratio of B-OH to (C-OH+Si-

OH), Table S4). Taking RTPP-3 as an example, a mixture containing PVA solution (6 ml, 50 mg/ml), TPB-3NH_2 solution (1 ml, 2.5 mg/ml), PDMS-OH (20 g, half high viscosity and half low viscosity), MeOH (2 ml) and BA (310 mg) was added to the beaker firstly. Subsequently, the mixture was stirred in an ambient environment for 4 h to get RTPP-3 prepolymer. Finally, the RTPP-3 prepolymer was dried under vacuum at 60 ℃ for 6 h to accomplish a complete B-O click reaction and remove the solvent.

The preparation process of DPCZ RTPP is consistent with RTPP-X, and the doping concentration of DPCZ is consistent with that of TPB-3NH_2 in RTPP-3.

The preparation of the silicon rubber/phosphor-doped PVA composite, a controlled sample, is similar to RTPP-X, except for replacing PDMS-OH with silicone rubber (Sylguard-184A: Sylguard-184B = 10:1).

Preparation of the multi-color afterglow putties

Firstly, fluorescent dyes RhB (20 mg) and Rh6G (20 mg) were dissolved in DMF (20 ml) to get an acceptor solution. Next, RhB (0.25 ml, 1 mg/ml) and Rh6G (0.25 ml, 1 mg/ml) were doped into donors RTPP-3 and DPCz RTPP prepolymer to get hybrid putties, respectively. Finally, the hybrid putties were dried under vacuum at 60 ℃ for 6 h to accomplish a complete B-O click reaction and remove the solvent, and labeled as RhB@TPB-3NH_2 Putty, Rh6G@TPB-3NH_2 Putty, RhB@DPCz Putty and Rh6G@DPCz Putty.

Measurements and Methods

Gel Permeation Chromatography (GPC). The molecular weight and polydispersity index (PDI) of PDMS-OH with different viscosity were measured on the Tosoh HIC-8320GPC at room temperature. Tetrahydrofuran (THF) as the eluent with a flow rate of 0.5 mL/min, where monodispersed polystyrene (PS) standard served to generate the calibration curves.

Rheology. Oscillatory frequency sweep tests were conducted on the MCR302 rheometer at a constant strain of 0.5 % by varying frequency 0.01–100 rad/s at 25 °C. The sample was a disk with a diameter of 8 mm and a thickness of 0.3 - 0.5 mm, and the tests were performed in the torsion mode.

Fourier transform infrared spectroscopy (FTIR). FTIR spectra were recorded using Nicolet iS10

(Nicolet, America) in the range of 4000-400 (650) cm^{-1} at room temperature.

X-ray Diffraction (XRD). The XRD of samples is carried out on a raku X-ray diffractometer (Ultima IV) equipped with a parallel beam optical device. The thickness of x % BA-PVA and x% BA-PBS were about 1 mm and 3 mm, respectively.

Steady-state and delayed PL spectra. The steady-state fluorescence and phosphorescence spectra of samples were collected on the HORIBA FluoroMax-4 spectrofluorometer. The thickness of samples was in the range of 1-3 mm.

Fluorescence lifetime. The fluorescence lifetime of TPB-3NH_2-doped x% BA-PVA, RTPP-X and DPCz RTPP were measured on a Fluorolog-3 spectrofluorometer (Horiba JobinYvon) with DeltaDiode (317 nm, DD-320) as the excitation source and a picosecond photon detection module (PPD-850) as the detector. The fluorescence lifetime of RhB@TPB-3NH_2 Putty, Rh6G@TPB-3NH_2 Putty, RhB@DPCz Putty and Rh6G@DPCz Putty were measured on a Fluorolog-3 spectrofluorometer (Horiba JobinYvon) with DeltaDiode (505 nm, DD-510) as the excitation source and a picosecond photon detection module (PPD-850) as the detector.

Phosphorescence lifetime. The phosphorescence lifetime of TPB-3NH_2-doped x% BA-PVA, RTPP-X and DPCz RTPP were measured on a Fluorolog-3 spectrofluorometer (Horiba JobinYvon) with SpectraLEDs (355 nm, S-355) as the excitation source and a picosecond photon detection module (PPD-850) as the detector. The phosphorescence lifetime of RhB@TPB-3NH_2 Putty, Rh6G@TPB-3NH_2 Putty, RhB@DPCz Putty and Rh6G@DPCz Putty were measured on a Fluorolog-3 spectrofluorometer (Horiba JobinYvon) with SpectraLEDs (535 nm, S-535) as the excitation source and a picosecond photon detection module (PPD-850) as the detector.

Quantum yields. Photoluminescence quantum yields (PLQY, ϕ_{PL}) were determined on a Fluorolog-3 spectrofluorometer (Horiba JobinYvon) with an integrating sphere (IS80, Labsphere) and a 450 W Xenon

Lamp as the excitation source and a CCD (SYNAPSE) as the detector.

Anti-impact test. The falling balls with different weights (11g, 15 g, 32 g, 64 g, and128 g) were dropped on ultra-thin glass (0.17 mm) covered with protective RTPP with different thicknesses (1.3 mm, 3.3 mm, 3.7 mm and 4.8 mm) from a height of 0.7 m (Figure S14A), respectively.

Density functional theory (DFT) Calculation. DFT calculations were performed with the ORCA 5.0.3 software package.[1] The geometry optimizations were performed using the B3LYP-D3(BJ) functional[2, 3] with the def2-SVP basis[4] was using for all atoms. TDDFT calculations were performed using the CAM-B3LYP functional[5] with the def2-SVP basis set[4] for all atoms. All calculations utilize the def2/J auxiliary basis.[6]

Molecular Dynamics (MD) Simulation. The partial charge of PVA, boric acid, crosslinked molecule and TPB molecule was calculated using Gaussian 16 code[7] and the 6-311g(d,p) basis functions were applied.[8] The generation amber force field (GAFF)[9] was used to parametrize all atoms of PVA, Boric acid Crosslinked molecule and TPB molecule, such as the bond parameters, angle parameters, dihedral angles, and so on. The effect of boric acid on the dihedral Angle distribution of TPB was studied by molecular dynamics (MD) simulation. In system 1 (TPB-3NH_2/ PVA with unreacted BA), 1 TPB molecule, 50 PVA molecules and 167 boric acids were randomly inserted into a cube box with a side length of 6.00 nm. In system 2 (TPB-3NH_2/BA-PVA), 1 TPB molecule，16 boric acid，2 PVA molecules and 39 crosslinked molecules were randomly inserted into a cube box with a side length of 6.00 nm. A 20 ns dynamic equilibrium simulation was carried out for the above two systems under the NPT ensemble, respectively (Figure S9). On this basis, a 20 ns dynamic equilibrium simulation was carried out under the NPT ensemble for data analysis. The MD simulations were performed in the GROMACS 2021 software package.[10-12] The steepest descent method was applied to minimize the initial energy for each system with a force tolerance of 1 kJ/(mol^{-1} nm^{-1}) and a maximum step size of 0.002 ps before MD calculations.[13] In all three directions, periodic boundary conditions were imposed. The Leapfrog algorithm was used to integrate the Newtonian equation of motion.[13] In NPT simulations, the

pressure was maintained at 1 bar by the Berendsen barostat in an isotropic manner, and the temperature was maintained by the V-rescale thermostat at 298.15 K.[14] The Particle-Mesh-Ewald (PME) with a fourth-order interpolation was used to evaluate the electrostatic interactions and a cutoff of 1.0 nm was employed to calculate the short-range van der Waals interactions.[15]

Afterglow images and videos. The samples were excited at 365 nm UV light from a 1400 mW LED lamp (UVGO, Zhongshan Zigu Lighting Electric Appliance Factory, Shanghai, China) at ambient conditions. The photo-activated time was about 2 s. After the UV lamp was turned off, the camera (iPhone 12pro) started to record the videos or images immediately.

Additional Discussions

Molecular chain motion in three mechanical states of polymers. From the polymer's physical point of view, there are three physical states of the polymer, namely, the viscous flow state, the rubber state and the glassy state. Generally, the mechanical state of polymers at room temperature (R.T.) is distinguished according to the glass transition temperature and the viscous flow temperature, namely T_g and T_f.[16] **For the glassy state** (Tg lower than R.T.), which is the state of most plastics at room temperature. As Figure $S1A_1$ shows, molecular chains under a glassy state are densely surrounded by their neighbors and their trajectories are severely limited by the crowding, showing a 'random coil' structure.[17] The movement of chain segments is apparently constrained in a virtual cage formed by its neighbors, which can be considered as compressed blobs (Figure $S1A_2$).[18] Thus, chain motions under the glassy state are characterized by localized secondary relaxation (β- and γ- relaxation, relaxation of side chains or motion of more rigid units, e.g., rotation and flipping of side groups) (Figure $S1B_2$)[19, 20]. At the same time, large-scale structural rearrangement due to α-modes is strongly inhibited (α-modes are considered as local density fluctuations at the molecular scale).[21] **For the rubbery state**, which is the state of most hydrogels and elastomers with covalent or non-covalent cross-linking and topological entanglement, and the essence of its molecular motion is the transition between the freezing of the chain segment and the free activity of the chain segment.[22] As Figure $S1B_1$ shows, cooperative segmental motion allows complete relaxation of the confined backbone conformation (from A to A'), as well as the secondary relaxation. **For the viscous flow state**, the essence of its molecular motion is the whole molecular chain changes

between freezing and freedom; that is, the whole chain can flow freely (Figure S1C$_1$, from A to A'). Such free chain motion, also known as chain slippage, that accompanied by the center-of-mass diffusion (Figure S1C$_2$, from M to M').[23] Moreover, it is well known that the more rigid chain structure is more conducive to a longer RTP lifetime.[24] Therefore, as Scheme. 1 shown (***Manuscript, Scheme. 1***), RTP plastics (PVA, PS, PMMA.et al.) under glassy state have a longer lifetime than hydrogels and elastomers under rubbery state generally (Table S5). Notably, putties under viscous flow state with free chain motion are indeed unfavorable to stable phosphor triplet, marking that the long RTP lifetimes (up to 2.39 s) of DPCz RTPP achieved in this work are really challenging and meaningful.

PBS/phosphor-doped PVA composites by solvent mixing or twin rollers technique. As mentioned in the manuscript (Manuscript, Introduction Section), it is a big challenge to realize RTP emission in polymer with fully flowing chains due to the inherent contradiction between high chain movement ability and high-efficiency phosphorescence emission. To fill this gap, heterogeneously doping PVA in PBS with free chain motion is a promising strategy to arrest the dynamics and the vibrational dissipation of the phosphors, further endowing PBS with RTP emission. However, it is well known that PDMS with a non-polar siloxane backbone is difficult to compatible with carbon chain polymer, especially PVA as a typical polar polymer. The huge polarity difference between PVA and PDMS leads to the phase separation as shown in Figure S3A., an obvious phase-separation line. Firstly, we would like to make forced PVA compatible with PDMS in a thermodynamic way. After preparing PBS and phosphor-doped PVA, respectively, we tried to fabricate PBS/phosphor-doped PVA composites by twin rollers technique under different temperatures (30 °C, 60 °C, 90 °C, 120 °C). The results showed that the compatibility between PVA and PDMS was still poor, even in the presence of a shear force field and thermal field (Figure S3B). Secondly, we tried to prepare PBS/phosphor-doped PVA composites by dissolving PBS in solvent (THF) and adding PVA and phosphor solution. Unfortunately, after removing the solvent, there was still an apparent phase separation (Figure S3C). Finally, we tried to use silicone rubber as the matrix; that is, Sylguard-184A, Sylguard-184, PVA and phosphor solution were mixed and then cured at 60 °C to obtain Silicon rubber/phosphor-doped PVA composite. There was no large block of PVA aggregate separated from the silicon rubber matrix in the composite, but it showed an opaque appearance

of milky white (Figure S3D), which indicated the phase separation of PVA and silicone rubber at the micro level.

Supporting Figures

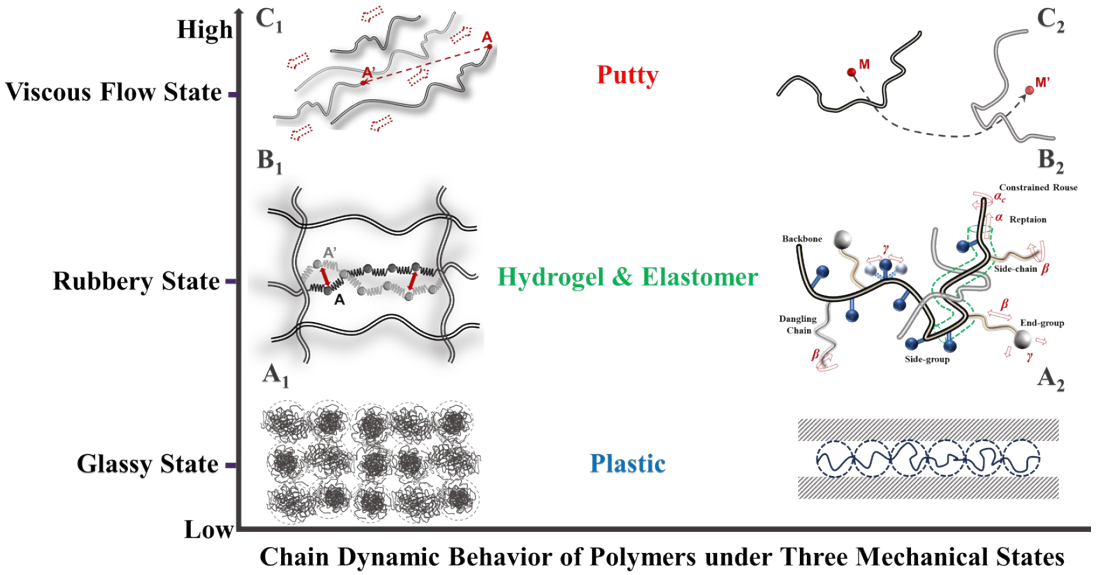

Figure S1. Molecular chain motion in three mechanical states of polymers.

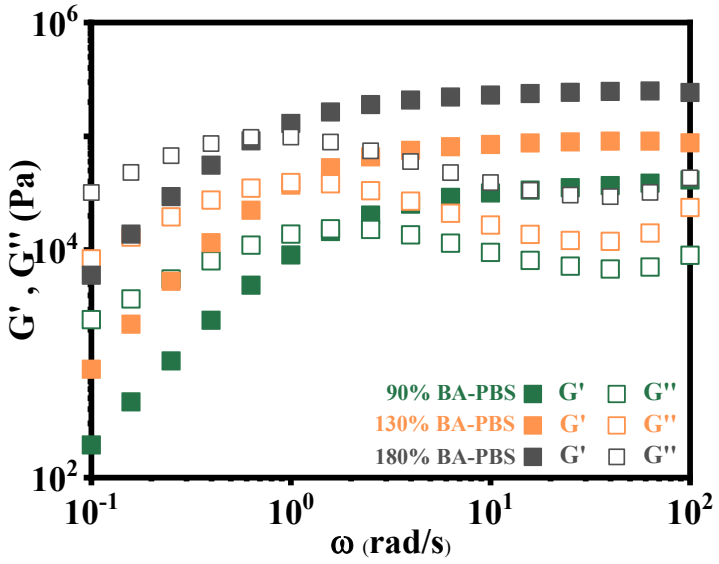

Figure S2. The effect of BA content on the viscoelastic properties of PBS: Dynamic storage (G′) and loss (G″) moduli of 90 % BA-PBS, 130 % BA-PBS and 180 % BA-PBS.

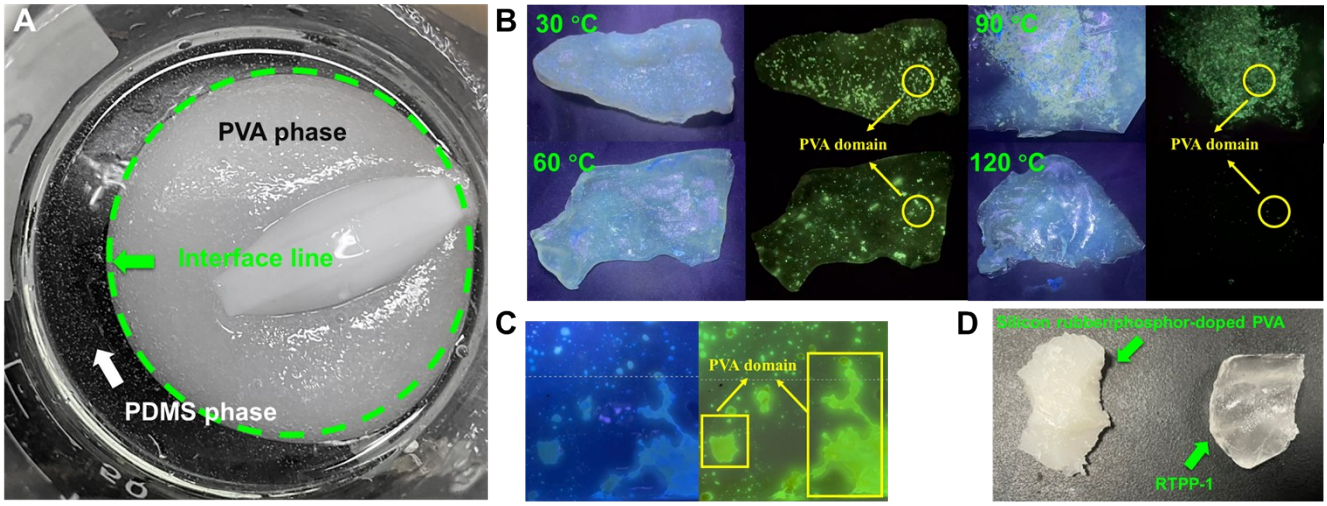

Figure S3. PBS/phosphor-doped PVA composites by solvent mixing or twin rollers technique. (**A**) Immiscibility between polar PVA and non-polar siloxane backbone; (**B**) PBS/phosphor-doped PVA composites by twin rollers technique under different temperatures (30 °C, 60 °C, 90 °C, 120 °C). There is a clear phase separation, where the RTP emission regions are the PVA phase domains; (**C**) PBS/phosphor-doped PVA composites by solvent mixing method. There is a clear phase separation, where the RTP emission regions are the PVA phase domains; (**D**) Silicon rubber/phosphor-doped PVA composites by solvent mixing.

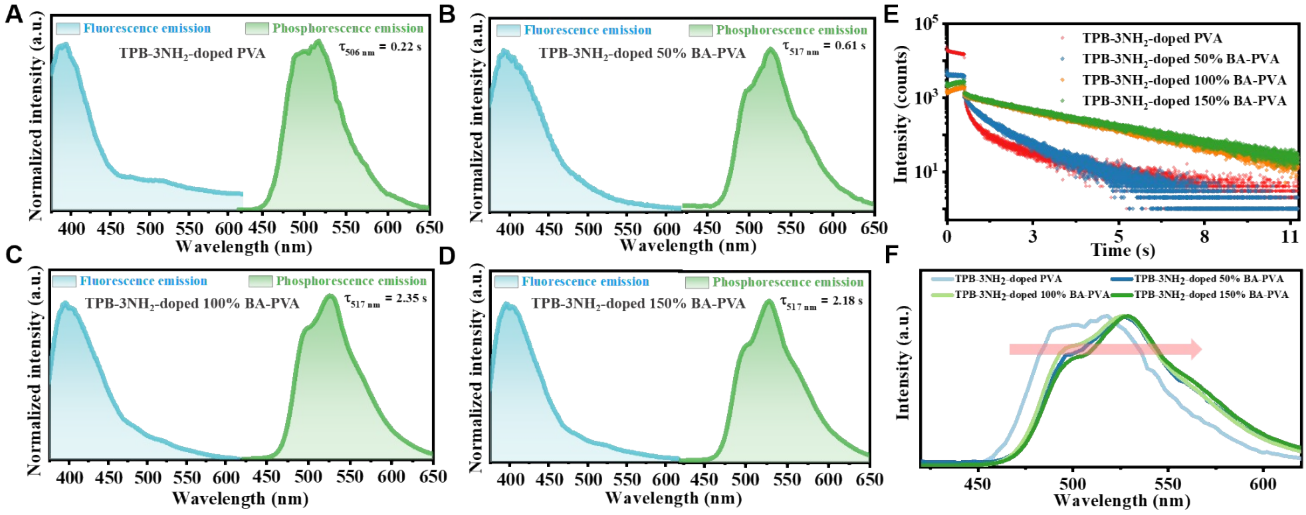

Figure S4. Effect of BA on the photophysical properties of TPB-3NH_2-doped x% BA-PVA. (**A**)-(**D**) Fluorescence and phosphorescence spectra and (**E**) Lifetime decay curves of TPB-3NH_2-doped X% BA-PVA (X = 0, 50, 100, 150); (**F**) A comparison of the phosphorescence emission spectra before and after the addition of BA shows that there is a significant redshift after the addition of BA, which is attributed to an increased restriction of the TPB-3NH_2 molecule by the BA-crosslinking PVA chains. The photoluminescence quantum yields (PLQY, ϕ_{PL}) of TPB-3NH_2-doped x% BA-PVA are summarized in Table S6.

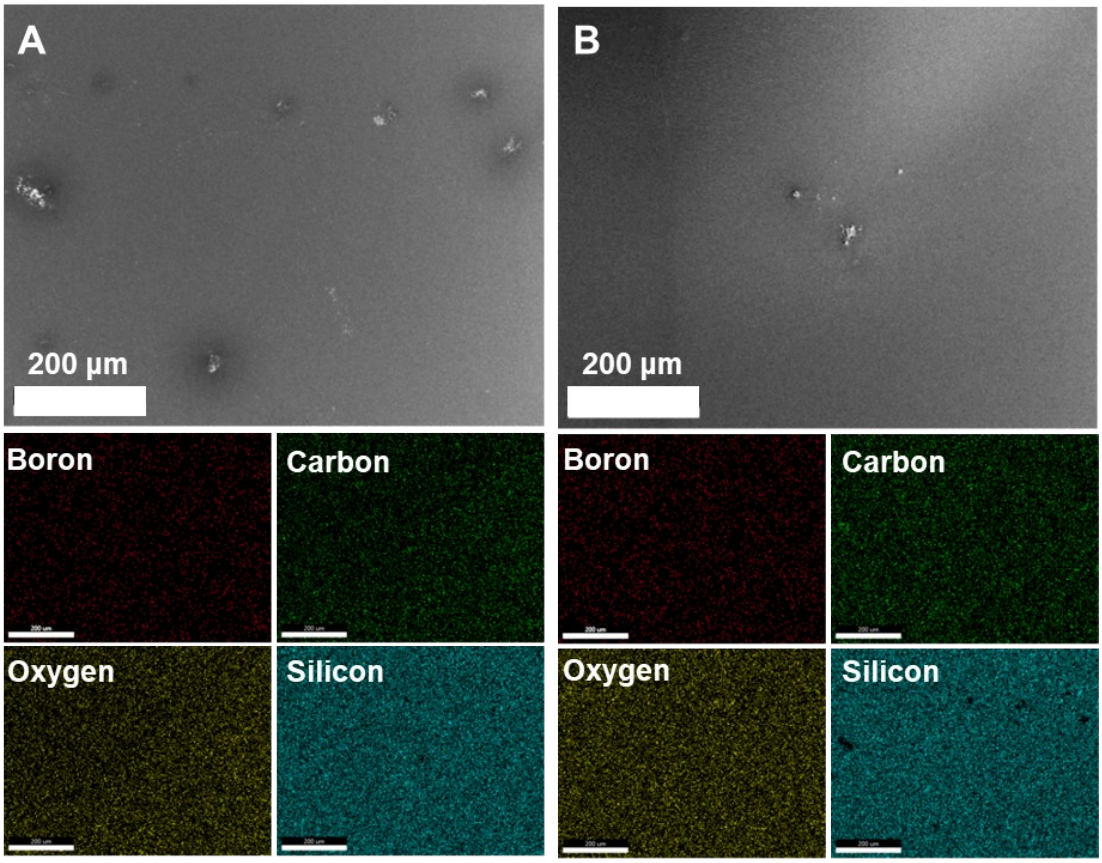

Figure S5. The SEM properties of RTPP-1 and RTPP-3. (**A**) SEM image and EDS images of RTPP-1 fracture section; (**B**) SEM image and EDS images of RTPP-3 fracture section.

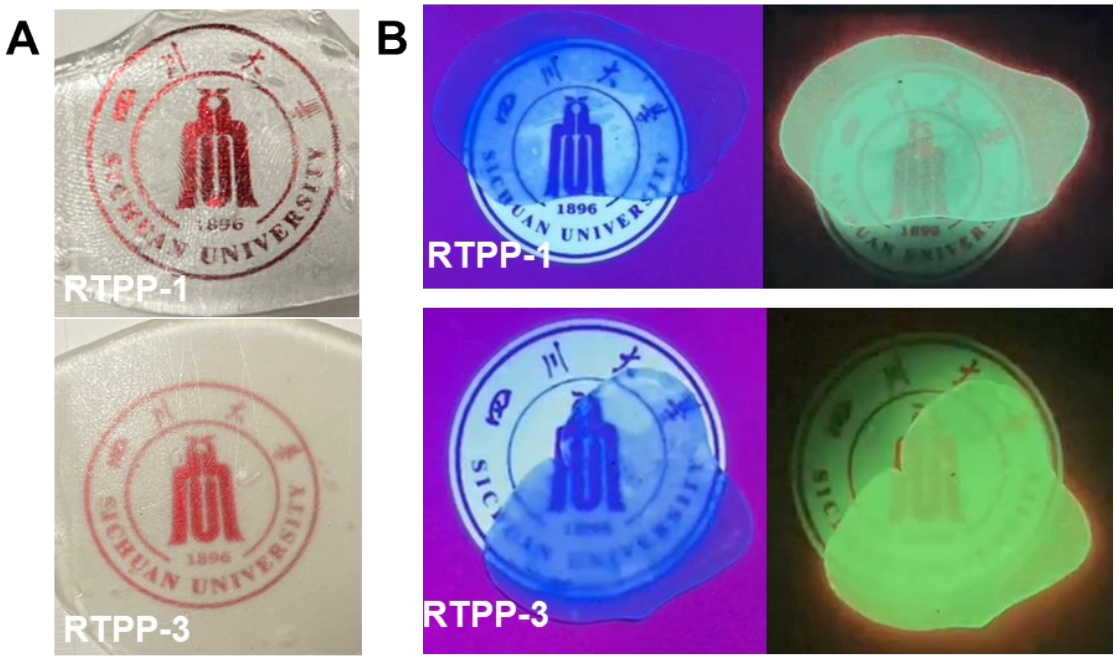

Figure S6. The transparent appearance and uniform emission of RTPP at the macro level. (**A**) Transparent appearance and (**B**) uniformly emission of RTPP-1 and RTPP-3.

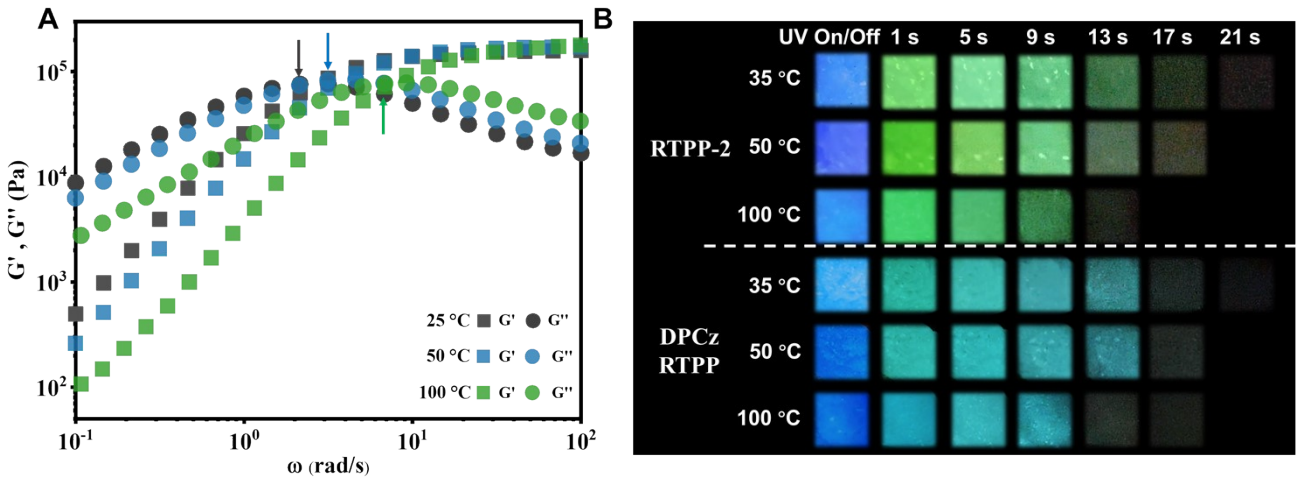

Figure S7. Mechanical characteristics and photophysical properties of RTPP-2 as a function of temperature. (**A**) Variable-temperature rheological test of RTPP, where the "solid-liquid" transition point of RTPP shifts to higher frequencies with increasing temperature. Such results suggest that RTPP exhibits a more liquid-like state with elevated temperatures; (**B**) Afterglow times of RTPP and DPCz RTPP at different temperatures. RTPP still retains RTP properties with enhanced fluidity property at high temperatures.

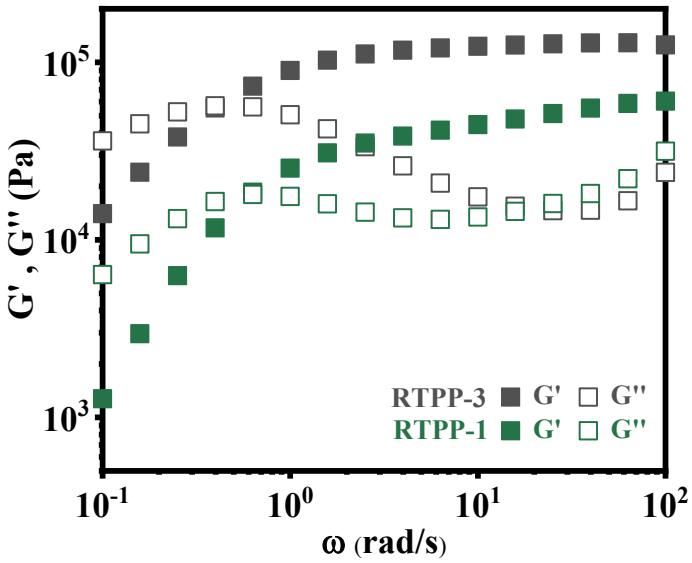

Figure S8. The effect of BA content on the viscoelastic properties of RTPP. Dynamic storage (G′) and loss (G″) moduli of RTPP-1 and RTPP-3. The crossover (G'=G'', ω_0) could give the terminal relaxation time ($\tau_d = 1/\omega_0$) of the RTPP, which is related to the rate of dynamic association and disassociation of boron ester bonds. Compared to RTPP-1, the G′ value of RTPP-3 increased, and the ω0 shifted to a lower frequency, proving that increased BA content can endow the dynamic network of RTPP with a higher limitation degree and lower chain exchange reaction degree.

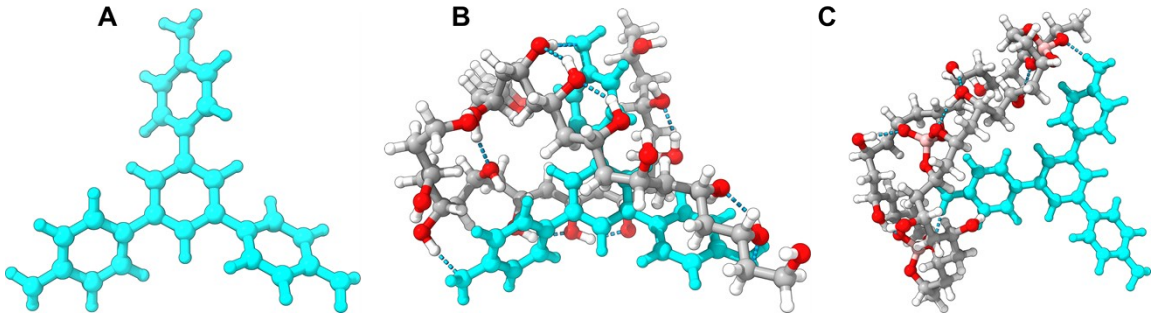

Figure S9. Optimized ground-state (S_0) geometries of (**A**) TPB-3NH_2 single-molecule, (**B**) TPB-3NH_2/PVA and (**C**) TPB-3NH_2/BA-PVA systems.

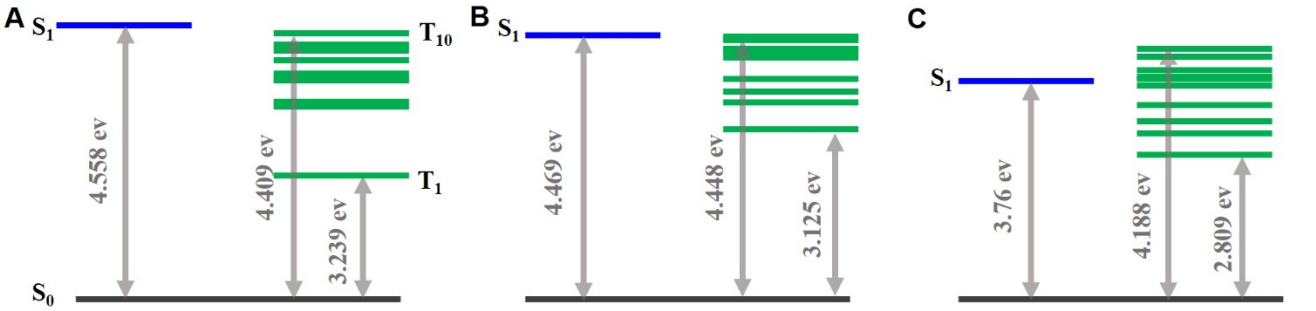

Sn	TPB-3NH_2	TPB-3NH_2/PVA	TPB-3NH_2/BA-PVA	Tn	TPB-3NH_2	TPB-3NH_2/PVA	TPB-3NH_2/BA-PVA
S_1	4.558	4.469	3.76	T_1	3.239	3.125	2.809
S_2	4.865	4.58	4.044	T_2	3.556	3.525	3.199
S_3	4.867	4.773	4.202	T_3	3.558	3.679	3.312
S_4	4.903	4.852	4.343	T_4	3.896	3.796	3.49
S_5	4.998	4.958	4.516	T_5	3.897	4.014	3.719
S_6	5	5.057	4.645	T_6	3.899	4.046	3.79
S_7	5.013	5.278	4.665	T_7	4.161	4.054	3.805
S_8	5.524	5.432	4.82	T_8	4.275	4.115	3.955
S_9	5.53	5.63	4.925	T_9	4.276	4.299	4.073
S_{10}	6.091	5.715	5.05	T_{10}	4.409	4.448	4.188

Figure S10. The energy level diagrams involved S_n and T_n states of (**A**) TPB-3NH_2 single-molecule, (**B**) TPB-3NH_2/PVA and (**C**) TPB-3NH_2/BA-PVA systems.

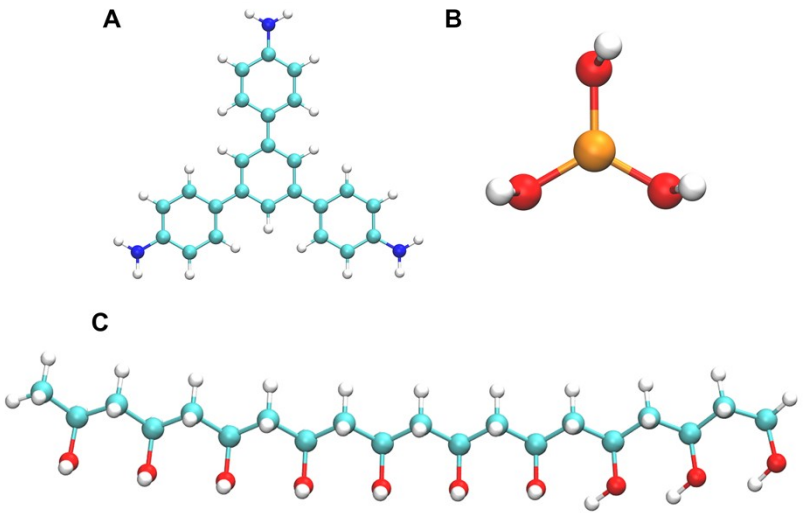

Figure S11. Optimized molecular conformation for molecular dynamics simulation: (**A**) TPB-3NH_2, (**B**) Boric acid and (**C**) PVA.

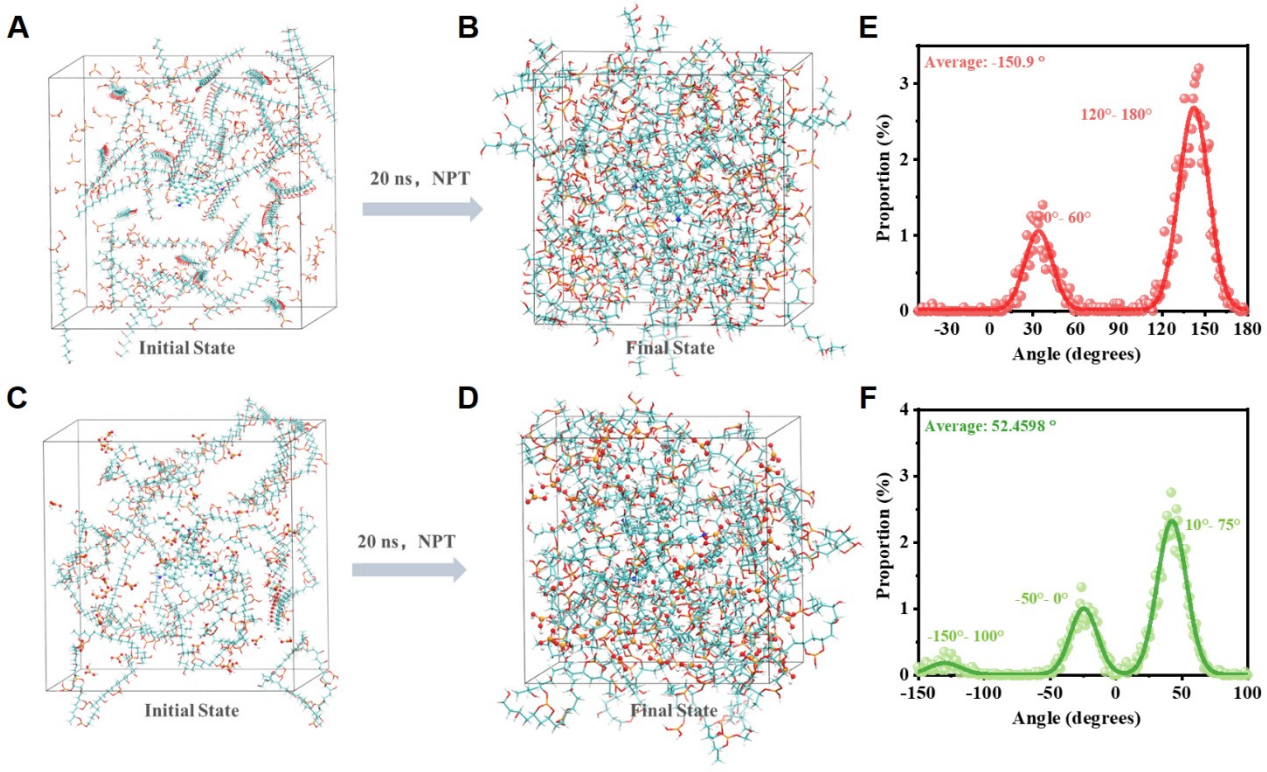

Figure S12. Molecular dynamics simulation snapshot of system 1 at (**A**) initial state and (**B**) final state, system 2 at (**C**) initial state and (**D**) final state, respectively. The dihedral angle (d) between the adjacent phenyl ring core of (**E**) system 1 and (**F**) system 2, the scatter points are original data, and the solid lines are Gaussian fit curves.

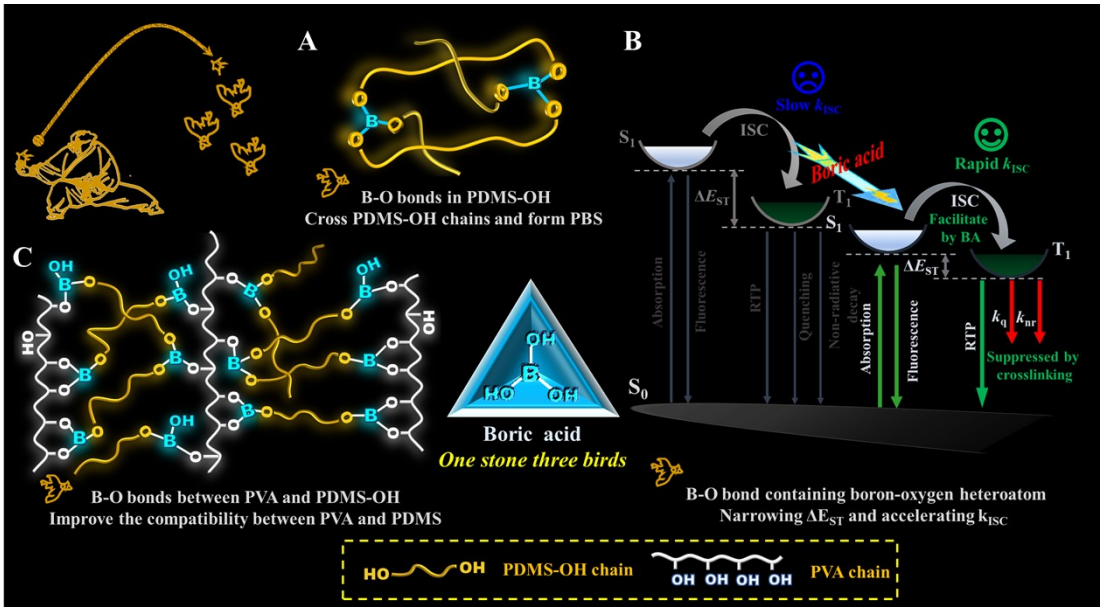

Figure S13. Illustration for the role of BA as "one stone three birds". (**A**) **Bird one:** BA can dynamically cross-link PDMS-OH chains to form PBS and regulate the rigidity of the PBS matrix; (**B**) **Bird two:** The underlying reason for ultralong-lived ambient RTP emission, that is B-O heteroatom can facilitate the intersystem crossing (ISC) via the formation of n-p* conjugate system induced by boron atom bearing a vacancy p orbital; (**C**) **Bird three:** The origin of the uniform phosphorescence can be attributed to the abundant B-O linkage in the interface phase, which alleviates the immiscibility between hydrophilic PVA and hydrophobic PBS.

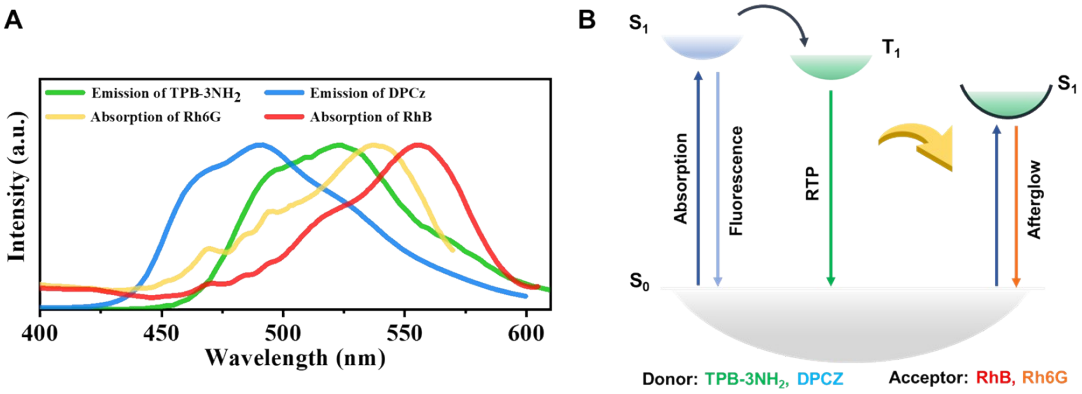

Figure S14. Design and mechanism of color-tunable fluorescence using the triplet-to-singlet Förster-resonance energy transfer (TS-FRET) strategy. (**A**) Fluorescence emission spectra of TPB-3NH_2 and DPCZ and absorption spectra of RhB and Rh6G, in which Rh6G and RhB with good spectral overlap with the TPB-3NH_2 and DPCz triplet emission were selected as the acceptors (**B**) Mechanism of the TS-FRET process, the triple state (T) energy of TPB-3NH_2 and DPCz could be transferred to the singlet state (S) of RhB and Rh6G through the T-S energy transfer process, then the singlet state excitons of RhB and Rh6G returned to the S_0 in the form of fluorescence emission, realizing a red-shift afterglow emission.

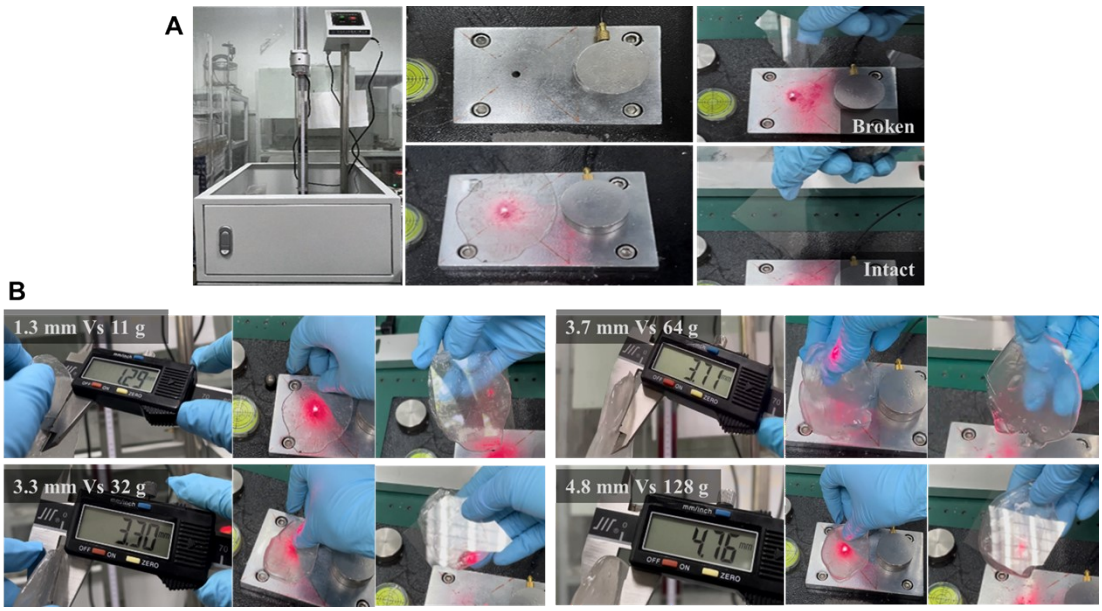

Figure S15. Anti-impact performance of RTPP. (**A**) Illustration of an impact protection test, RTPP protected the glass from breaking; (B) Anti-impact property of RTPP with various thicknesses against iron balls of different weights, showing that RTPP effectively protected the glass from breaking. Notably, the RTPP, with a thickness of 1.3 mm, can fully absorb the impact force caused by the 11 g iron ball.

Supporting Tables

Table S1. The raw materials feeding ratios of x% BA-PBS.

	90% BA-PBS	130% BA-PBS	180% BA-PBS
B-OH : Si-OH	9 : 10	13 : 10	18 : 10
High viscosity PDMS-OH / g*	10	10	10
Low viscosity PDMS-OH**	10	10	10
BA / g	0.10	0.14	0.20

* The molecular weight and polydispersity index (PDI) of high viscosity PDMS-OH are 73648 g/mol and 1.36 g/mol, respectively.

**The molecular weight and polydispersity index (PDI) of low viscosity PDMS-OH are 3894 and 1.27, respectively.

Table S2. The raw materials feeding ratios of x% BA-PVA.

	50% BA-PVA	100% BA-PVA	150% BA-PVA
B-OH : C-OH	5 : 10	100 : 100	150 : 100
PVA	0.5	0.5	0.5
BA / g	0.12	0.23	0.35

Table S3. The raw materials feeding ratios of TPB-3NH_2-doped x% BA-PVA.

TPB-3NH_2-doped	PVA	50% BA-PVA	100% BA-PVA	150% BA-PVA
TPB-3NH_2 / mg	1	1	1	1
PVA / g	0.5	0.5	0.5	0.5
BA / g	0	0.12	0.23	0.35

Table S4. The raw materials feeding ratios of RTPP-X.

	RTPP-1	RTPP-2	RTPP-3	RTPP-4
B-OH : (Si-OH+C-OH)	0.75	1	1.25	1.5
TPB-3NH_2 / mg	2.5	2.5	2.5	2.5
PVA / g	0.3	0.3	0.3	0.3
High viscosity PDMS-OH / g*	10	10	10	10
Low viscosity PDMS-OH**	10	10	10	10
BA / g	0.19	0.25	0.31	0.38

Glassy State			Rubbery State		
Time[Ref.]	Author	Lifetime (s) *	Time[Ref.]	Author	Lifetime (s) *
(2021)[25]	Zhao's work	0.83	**(2022)[26]**	Chi's work	0.78
(2021)[27]	Zhao's work	2.04	**(2023)[28]**	Li's work	0.54
(2014)[29]	Kim's work	4.70E-03	**(2021)[30]**	George's work	1.62E-04
(2023)[31]	Lu's work	1.45	**(2020)[32]**	He's work	1.90E-04
(2018)[33]	Ogoshi's work	1.22	**(2022)[34]**	Yang's work	0.83
(2018)[35]	Adachi's work	1.09	**(2023)[36]**	Yang's work	1.22
(2021)[37]	Xie's work	2.16	**(2023)[38]**	Huang's work	0.79
(2020)[39]	Liu's work	2.81	**(2023)[40]**	Wu' work	0.34
(2022)[41]	Li's work	2.43	**(2021)[42]**	Huang's work	0.48
(2023)[43]	Peng's work	1.42	**(2014)[44]**	Tian's work	0.56
(2023)[45]	Huang's work	0.87	**(2016)[46]**	Tian's work	3.20E-04
(2022)[47]	Li's work	2.43	**(2021)[48]**	Liu's work	1.24E-03
(2018)[49]	Zhao's work	0.75	**(2020)[50]**	Ma's work	8.30E-05
(2020)[51]	Lu's work	0.77	**(2015)[52]**	Kimizuka's work	2.28E-04
(2019)[53]	Huang's work	2.1	**(2020)[54]**	Yang's work	2.05E-03
(2020)[55]	Yuan's work	1.04	**(2019)[56]**	Liu's work	2.79E-03
(2022)[57]	Liang's work	0.75	**(2024)[58]**	Huang's work	0.98
(2023)[59]	Yang's work	0.24	**(2024)[60]**	Wen'work	0.63
(2020)[61]	Zhao's work	1.2	**(2024)[62]**	Gu's work	0.72
(2018)[63]	Qu's work	2.00E-07	**(2024)[64]**	He's work	1.99E-03
(2016)[65]	Tian's work	5.76E-03			
(2013)[66]	Kim's work	2.15E-03			
(2015)[67]	Kim's work	2.60E-03	**Viscous Flow State**		
(2024)[68]	Yang's work	0.95			
(2024)[69]	Yang's work	5.82			
(2024)[70]	Ma's work	4.18			
(2024)[71]	Zhong's work	1.5		This work	2.39
(2024)[72]	Ma's work	1.92			
(2023)[73]	Yang's work	1.8			
(2023)[74]	Zhang's work	2.4			

Table S5. The RTP lifetimes reported by previous works.

*Selecting the sample with the longest lifetime in the same work.

Table S6. The ϕ_{PL} of TPB-3NH_2-doped x% BA-PVA and RTPP-X

Samples		ϕ_{PL}	Samples		ϕ_{PL}
TPB-3NH_2-doped	PVA	11.39%	RTPP-X	RTPP-1	8.12%
	50% BA-PVA	5.55%		RTPP-2	14.29%
	100% BA-PVA	10.51%		RTPP-3	5.34%
	150% BA-PVA	10.55%		RTPP-4	8.98%

Table S7. The ϕ_{PL} of multi-color afterglow putties

Samples	ϕ_{PL}
DPCz RTPP	8.49%
RhB@TPB-3NH_2 Putty	28.85%
RhB@DPCz Putty	43.79%
Rh6G@TPB-3NH_2 Putty	16.95%
Rh6G@DPCz Putty	18.91%

Legends for Movies S1 to S8

Movie S1. RTP Afterglow Emission of RTPP-3

Movie S2. RTP Afterglow Emission of DPCz RTPP

Movie S3. Self-healing Behavior of RTPP

Movie S4. The Tailorability of RTPP

Movie S5. The Repeated Molding Demonstration of RTPP

Movie S6. The Solid-liquid Behavior of RTPP

Movie S7. The Elastic Demonstration of RTPP

Movie S8. The Anti-impact Performance of RTPP

References

1. F. Neese, F. Wennmohs, U. Becker and C. Riplinger, *The Journal of Chemical Physics*, 2020, **152**, 224108.
2. G. J. Hoffman, D. G. Imre, R. Zadoyan, N. Schwentner and V. A. Apkarian, *The Journal of Chemical Physics*, 1993, **98**, 9233-9240.
3. A. D. Becke, *The Journal of Chemical Physics*, 1992, **96**, 2155-2160.
4. F. Weigend and R. Ahlrichs, *Physical Chemistry Chemical Physics*, 2005, **7**, 3297-3305.
5. T. Yanai, D. P. Tew and N. C. Handy, *Chemical Physics Letters*, 2004, **393**, 51-57.
6. F. Weigend, *Physical Chemistry Chemical Physics*, 2006, **8**, 1057-1065.
7. M. J. Frisch, G. W. Trucks, H. B. Schlegel, G. E. Scuseria, M. A. Robb, J. R. Cheeseman, G. Scalmani, V. Barone, G. A. Petersson, H. Nakatsuji, X. Li, M. Caricato, A. V. Marenich, J. Bloino, B. G. Janesko, R. Gomperts, B. Mennucci, H. P. Hratchian, J. V. Ortiz, A. F. Izmaylov, J. L. Sonnenberg, Williams, F. Ding, F. Lipparini, F. Egidi, J. Goings, B. Peng, A. Petrone, T. Henderson, D. Ranasinghe, V. G. Zakrzewski, J. Gao, N. Rega, G. Zheng, W. Liang, M. Hada, M. Ehara, K. Toyota, R. Fukuda, J. Hasegawa, M. Ishida, T. Nakajima, Y. Honda, O. Kitao, H. Nakai, T. Vreven, K. Throssell, J. A. Montgomery Jr., J. E. Peralta, F. Ogliaro, M. J. Bearpark, J. J. Heyd, E. N. Brothers, K. N. Kudin, V. N. Staroverov, T. A. Keith, R. Kobayashi, J. Normand, K. Raghavachari, A. P. Rendell, J. C. Burant, S. S. Iyengar, J. Tomasi, M. Cossi, J. M. Millam, M. Klene, C. Adamo, R. Cammi, J. W. Ochterski, R. L. Martin, K. Morokuma, O. Farkas, J. B. Foresman and D. J. Fox, *Journal*, 2016.
8. G. A. Petersson and M. A. Al‐Laham, *The Journal of Chemical Physics*, 1991, **94**, 6081-6090.
9. J. Wang, R. M. Wolf, J. W. Caldwell, P. A. Kollman and D. A. Case, *Journal of Computational Chemistry*, 2004, **25**, 1157-1174.
10. D. Van Der Spoel, E. Lindahl, B. Hess, G. Groenhof, A. E. Mark and H. J. C. Berendsen, *Journal of Computational Chemistry*, 2005, **26**, 1701-1718.
11. M. J. Abraham, T. Murtola, R. Schulz, S. Páll, J. C. Smith, B. Hess and E. Lindahl, 2015, **1-2**.
12. H. J. C. Berendsen, D. van der Spoel and R. van Drunen, *Computer Physics Communications*, 1995, **91**, 43-56.
13. W. F. Van Gunsteren and H. J. C. Berendsen, *Molecular Simulation*, 1988, **1**, 173-185.
14. B. Hess, H. Bekker, H. J. C. Berendsen and J. G. E. M. Fraaije, *Journal of Computational Chemistry*, 1997, **18**, 1463-1472.
15. T. Darden, D. York and L. Pedersen, *The Journal of Chemical Physics*, 1993, **98**, 10089-10092.
16. D. Cangialosi, *Journal of Physics: Condensed Matter*, 2014, **26**, 153101.
17. G. Adam and J. H. Gibbs, *The Journal of Chemical Physics*, 2004, **43**, 139-146.
18. Y. Yang, Q. Xu, T. Jin, X. Wang, S. Napolitano and B. Zuo, *Macromolecules*, 2023, **56**, 5924-5931.
19. J. Xu, J. Chen, Y. Zhang, T. Liu and J. Fu, *Angewandte Chemie International Edition*, 2021, **60**, 7947-7955.
20. H. Wang, H. Liu, Z. Cao, W. Li, X. Huang, Y. Zhu, F. Ling, H. Xu, Q. Wu, Y. Peng, B. Yang, R. Zhang, O. Kessler, G. Huang and J. Wu, *Proceedings of the National Academy of Sciences*, 2020, **117**, 11299-11305.
21. S. Napolitano, E. Glynos and N. B. Tito, *Reports on Progress in Physics*, 2017, **80**, 036602.
22. L. Zhang, H. Wang, Y. Zhu, H. Xiong, Q. Wu, S. Gu, X. Liu, G. Huang and J. Wu, *ACS Applied Materials & Interfaces*, 2020, **12**, 53239-53246.
23. N. Jiang, H. Zhang, P. Tang and Y. Yang, *Macromolecules*, 2020, **53**, 3438-3451.
24. W. Zhao, Z. He and B. Z. Tang, *Nature Reviews Materials*, 2020, **5**, 869-885.
25. Y. Zhang, L. Gao, X. Zheng, Z. Wang, C. Yang, H. Tang, L. Qu, Y. Li and Y. Zhao, *Nature Communications*, 2021, **12**, 2297.
26. Z. Sun, H. Deng, Z. Mao, Z. Li, K. Nie, K. Fu, J. Chen, J. Zhao, P. Zhu, Z. Chi and R. Sun, *Advanced Optical*

Materials, 2022, **10**, 2201558.
27. Y. Zhang, Y. Su, H. Wu, Z. Wang, C. Wang, Y. Zheng, X. Zheng, L. Gao, Q. Zhou, Y. Yang, X. Chen, C. Yang and Y. Zhao, *Journal of the American Chemical Society*, 2021, **143**, 13675-13685.
28. Z.-H. Zhao, P.-C. Zhao, S.-Y. Chen, Y.-X. Zheng, J.-L. Zuo and C.-H. Li, *Angewandte Chemie International Edition*, 2023, **62**, e202301993.
29. M. S. Kwon, D. Lee, S. Seo, J. Jung and J. Kim, *Angewandte Chemie International Edition*, 2014, **53**, 11177-11181.
30. S. Garain, B. C. Garain, M. Eswaramoorthy, S. K. Pati and S. J. George, *Angewandte Chemie International Edition*, 2021, **60**, 19720-19724.
31. R. Tian, S. Gao, K. Li and C. Lu, *Nature Communications*, 2023, **14**, 4720.
32. J. Wang, Z. Huang, X. Ma and H. Tian, *Angewandte Chemie International Edition*, 2020, **59**, 9928-9933.
33. T. Ogoshi, H. Tsuchida, T. Kakuta, T.-a. Yamagishi, A. Taema, T. Ono, M. Sugimoto and M. Mizuno, *Advanced Functional Materials*, 2018, **28**, 1707369.
34. Y. Zhang, Q. Sun, L. Yue, Y. Wang, S. Cui, H. Zhang, S. Xue and W. Yang, *Advanced Science*, 2022, **9**, 2103402.
35. Z. Lin, R. Kabe, N. Nishimura, K. Jinnai and C. Adachi, *Advanced Materials*, 2018, **30**, 1803713.
36. J. Chen, Y. Zhang, S. Zhang, G. Liu, Q. Sun, S. Xue and W. Yang, *Small Structures*, 2023, **4**, 2300101.
37. Y. Zhu, Y. Guan, Y. Niu, P. Wang, R. Chen, Y. Wang, P. Wang and H.-L. Xie, *Advanced Optical Materials*, 2021, **9**, 2100782.
38. J. Wei, M. Zhu, T. Du, J. Li, P. Dai, C. Liu, J. Duan, S. Liu, X. Zhou, S. Zhang, L. Guo, H. Wang, Y. Ma, W. Huang and Q. Zhao, *Nature Communications*, 2023, **14**, 4839.
39. Z.-Y. Zhang, W.-W. Xu, W.-S. Xu, J. Niu, X.-H. Sun and Y. Liu, *Angewandte Chemie International Edition*, 2020, **59**, 18748-18754.
40. H. Ju, H. Zhang, L. X. Hou, M. Zuo, M. Du, F. Huang, Q. Zheng and Z. L. Wu, *Journal of the American Chemical Society*, 2023, **145**, 3763-3773.
41. D. Li, Y. Yang, J. Yang, M. Fang, B. Z. Tang and Z. Li, *Nature Communications*, 2022, **13**, 347.
42. S. Cai, Z. Sun, H. Wang, X. Yao, H. Ma, W. Jia, S. Wang, Z. Li, H. Shi, Z. An, Y. Ishida, T. Aida and W. Huang, *Journal of the American Chemical Society*, 2021, **143**, 16256-16263.
43. Q. Gao, M. Shi, Z. Lü, Q. Zhao, G. Chen, J. Bian, H. Qi, J. Ren, B. Lü and F. Peng, *Advanced Materials*, 2023, **n/a**, 2305126.
44. H. Chen, X. Ma, S. Wu and H. Tian, *Angewandte Chemie International Edition*, 2014, **53**, 14149-14152.
45. H. Li, X. Xue, Y. Cao, H. Cheng, A. Luo, N. Guo, H. Li, G. Xie, Y. Tao, R. Chen and W. Huang, *Journal of the American Chemical Society*, 2023, **145**, 7343-7351.
46. H. Chen, L. Xu, X. Ma and H. Tian, *Polymer Chemistry*, 2016, **7**, 3989-3992.
47. D. Li, J. Yang, M. Fang, B. Z. Tang and Z. Li, *Science Advances*, **8**, eabl8392.
48. W.-T. Fan, Y. Chen, J. Niu, T. Su, J.-J. Li and Y. Liu, *Advanced Photonics Research*, 2021, **2**, 2000080.
49. Y. Su, S. Z. F. Phua, Y. Li, X. Zhou, D. Jana, G. Liu, W. Q. Lim, W. K. Ong, C. Yang and Y. Zhao, *Science Advances*, 2018, **4**, eaas9732.
50. T. Zhang, X. Ma and H. Tian, *Chemical Science*, 2020, **11**, 482-487.
51. R. Tian, S.-M. Xu, Q. Xu and C. Lu, *Science Advances*, 2020, **6**, eaaz6107.
52. P. Duan, N. Yanai, H. Nagatomi and N. Kimizuka, *Journal of the American Chemical Society*, 2015, **137**, 1887-1894.
53. S. Cai, H. Ma, H. Shi, H. Wang, X. Wang, L. Xiao, W. Ye, K. Huang, X. Cao, N. Gan, C. Ma, M. Gu, L. Song, H. Xu, Y. Tao, C. Zhang, W. Yao, Z. An and W. Huang, *Nature Communications*, 2019, **10**, 4247.
54. H. Wang, H. Wang, X. Yang, Q. Wang and Y. Yang, *Langmuir*, 2015, **31**, 486-491.
55. X. Dou, T. Zhu, Z. Wang, W. Sun, Y. Lai, K. Sui, Y. Tan, Y. Zhang and W. Z. Yuan, *Advanced Materials*, 2020, **32**,

2004768.
56. J.-J. Li, H.-Y. Zhang, Y. Zhang, W.-L. Zhou and Y. Liu, *Advanced Optical Materials*, 2019, **7**, 1900589.
57. W. Tao, Y. Zhou, F. Lin, H. Gao, Z. Chi and G. Liang, *Advanced Optical Materials*, 2022, **10**, 2102449.
58. N. Gan, X. Zou, Z. Qian, A. Lv, L. Wang, H. Ma, H.-J. Qian, L. Gu, Z. An and W. Huang, *Nature Communications*, 2024, **15**, 4113.
59. J. You, X. Zhang, Q. Nan, K. Jin, J. Zhang, Y. Wang, C. Yin, Z. Yang and J. Zhang, *Nature Communications*, 2023, **14**, 4163.
60. L. Qiu, Z. Chen, J. Wu, G. Zeng, X. Liu, K. Liu, S.-j. Su, J. Loos and T. Wen, *Macromolecules*, 2024, **57**, 2679-2686.
61. L. Gu, H. Wu, H. Ma, W. Ye, W. Jia, H. Wang, H. Chen, N. Zhang, D. Wang, C. Qian, Z. An, W. Huang and Y. Zhao, *Nature Communications*, 2020, **11**, 944.
62. H. Chen, Z. Qian, H.-J. Qian, M. Dong, Y. Zhang, J. Shan, W. Huo, A. Lv, J. Guo, H. Ma, Z. An, W. Huang and L. Gu, *Chemistry of Materials*, 2024, DOI: 10.1021/acs.chemmater.4c00307.
63. Z. Tian, D. Li, E. V. Ushakova, V. G. Maslov, D. Zhou, P. Jing, D. Shen, S. Qu and A. L. Rogach, *Advanced Science*, 2018, **5**, 1800795.
64. Y. Cao, D. Wang, Y. Zhang, G. Li, C. Gao, W. Li, X. Chen, X. Chen, P. Sun, Y. Dong, Z. Cai and Z. He, *Angewandte Chemie International Edition*, 2024, **63**, e202401331.
65. H. Chen, X. Yao, X. Ma and H. Tian, *Advanced Optical Materials*, 2016, **4**, 1397-1401.
66. D. Lee, O. Bolton, B. C. Kim, J. H. Youk, S. Takayama and J. Kim, *Journal of the American Chemical Society*, 2013, **135**, 6325-6329.
67. M. S. Kwon, Y. Yu, C. Coburn, A. W. Phillips, K. Chung, A. Shanker, J. Jung, G. Kim, K. Pipe, S. R. Forrest, J. H. Youk, J. Gierschner and J. Kim, *Nature Communications*, 2015, **6**, 8947.
68. J. Huang, L. Qu, L. Gao, X. Wang, Q. Chen, Y. Wang, Y. Zhu, C. Li, Y. Li and C. Yang, *Macromolecules*, 2024, DOI: 10.1021/acs.macromol.4c00021.
69. Y. Miao, F. Lin, D. Guo, J. Chen, K. Zhang, T. Wu, H. Huang, Z. Chi and Z. Yang, *Science Advances*, 2024, **10**, eadk3354.
70. K. Chen, Y. Zhang, Y. Lei, W. Dai, M. Liu, Z. Cai, H. Wu, X. Huang and X. Ma, *Nature Communications*, 2024, **15**, 1269.
71. D.-X. Ma, Z.-Q. Li, K. Tang, Z.-L. Gong, J.-Y. Shao and Y.-W. Zhong, *Nature Communications*, 2024, **15**, 4402.
72. L. Zhou, J. Song, Z. He, Y. Liu, P. Jiang, T. Li and X. Ma, *Angewandte Chemie International Edition*, 2024, **63**, e202403773.
73. C. Li, F. Guo, Y. Zhu, Q. Zhou, Q. Chen, Y. Wang, J. Huang, L. Qu and C. Yang, *Macromolecules*, 2023, **56**, 10028-10036.
74. Y. Zuo, H. Yang, K. Wang, Y. Song, L. Jiang, W. Huang, X. Xue, Q. Jiang, B. Jiang and G. Zhang, *Macromolecules*, 2023, **56**, 5854-5864.